Excitation nonlinearities in emission reabsorption laser-induced fluorescence techniques

Carlos H. Hidrovo, Ricardo R. Brau, and Douglas P. Hart

The effects of the nonlinear behavior of fluorescent intensity with excitation intensity on emission reabsorption laser-induced fluorescence (ERLIF) are investigated. Excitation nonlinearities arise mainly as a consequence of the depletion of the ground-state population stemming from the finite lifetime of molecules in the excited state. These nonlinearities hinder proper suppression of the excitation intensity information in the fluorescence ratio, degrading measurement accuracy. A method for minimizing this effect is presented. This method is based on the approximation of the fluorescence intensity nonlinearities by a power law. Elevating the two-dimensional fluorescent intensity maps to the appropriate exponent allows for proper suppression of excitation intensity in the fluorescence ratio. An overview of the principles and constitutive equations behind ERLIF film-thickness measurements, along with a characterization of the fluorescence's nonlinear behavior, is presented. The power law approximation and processing scheme used to mitigate this behavior are introduced. Experimental proof of the validity of the approximation and processing scheme is provided.

OCIS codes: 120.0120, 120.3940, 190.0190, 260.2510, 280.2490, 300.2530.

1. Introduction

Laser-induced fluorescence, a technique based on the photoexcitation of a fluorophore or a fluorescent dye, has been extensively used as a general-purpose display tool in one-, two-, and three-dimensional applications.[1,2] However, it is used mainly as a tracer for qualitative purposes[3–5] and has seen only limited use as a quantitative tool. This limitation stems primarily from the fact that fluorescent intensity is dependent on the intensity of the exciting light. Variations in exciting-light intensity, surface reflectivity, and optical distortion effects make fluorescence-based correlations (fluorescence calibrations) impractical if not impossible. By using two different fluorescent dyes and ratioing their emissions it is possible to eliminate exciting-light intensity information while preserving the information of interest.[6–8]

This approach was presented previously for film-thickness measurements in the form of emission reabsorption laser-induced fluorescence (ERLIF).[8] The idea is to take the ratio of two simultaneously captured fluorescent emission intensity maps to suppress excitation intensity information. To preserve film-thickness information in the ratio it is necessary for one of the fluorescent emissions to exhibit reabsorption. This ensures that the dependences of the fluorescent emissions on film thickness are different and will not cancel in the ratio. It has been demonstrated that ERLIF is capable of eliminating the uncertainty introduced by excitation intensity fluctuations for film-thickness measurements in the hundreds-of-micrometers range. A tangible example of the accuracy of the ERLIF technique is shown in Fig. 1. We used ERLIF here to infer the surface topography of a U.S. 25¢ coin. The coin was placed flat in the bottom of a beaker, and a small layer of oil premixed with two fluorescent dyes was deposited on top of the coin. We then used ERLIF to measure the film thickness of the oil on top of the coin. Because of the topography of the coin, the thickness of the oil film on top of the coin generated a female match of the coin features: raised surface regions produced a thin film (low fluorescence) and, vice versa, surface depressions produced a thick film (high fluorescence). Thus, one must invert the film-thickness profile to obtain the topography of the coin's surface. At the top of Fig. 1 are shown the two fluorescent emission images of the oil film lying on top of the coin. It is impossible to infer

The authors are with the Department of Mechanical Engineering, Massachusetts Institute of Technology, 77 Massachusetts Avenue, Cambridge, Massachusetts 02139. C. H. Hidrovo's e-mail address is hidrovo@stanford.edu.

Received 16 July 2003; revised manuscript received 16 July 2003; accepted 8 October 2003.

0003-6935/04/040894-20$15.00/0

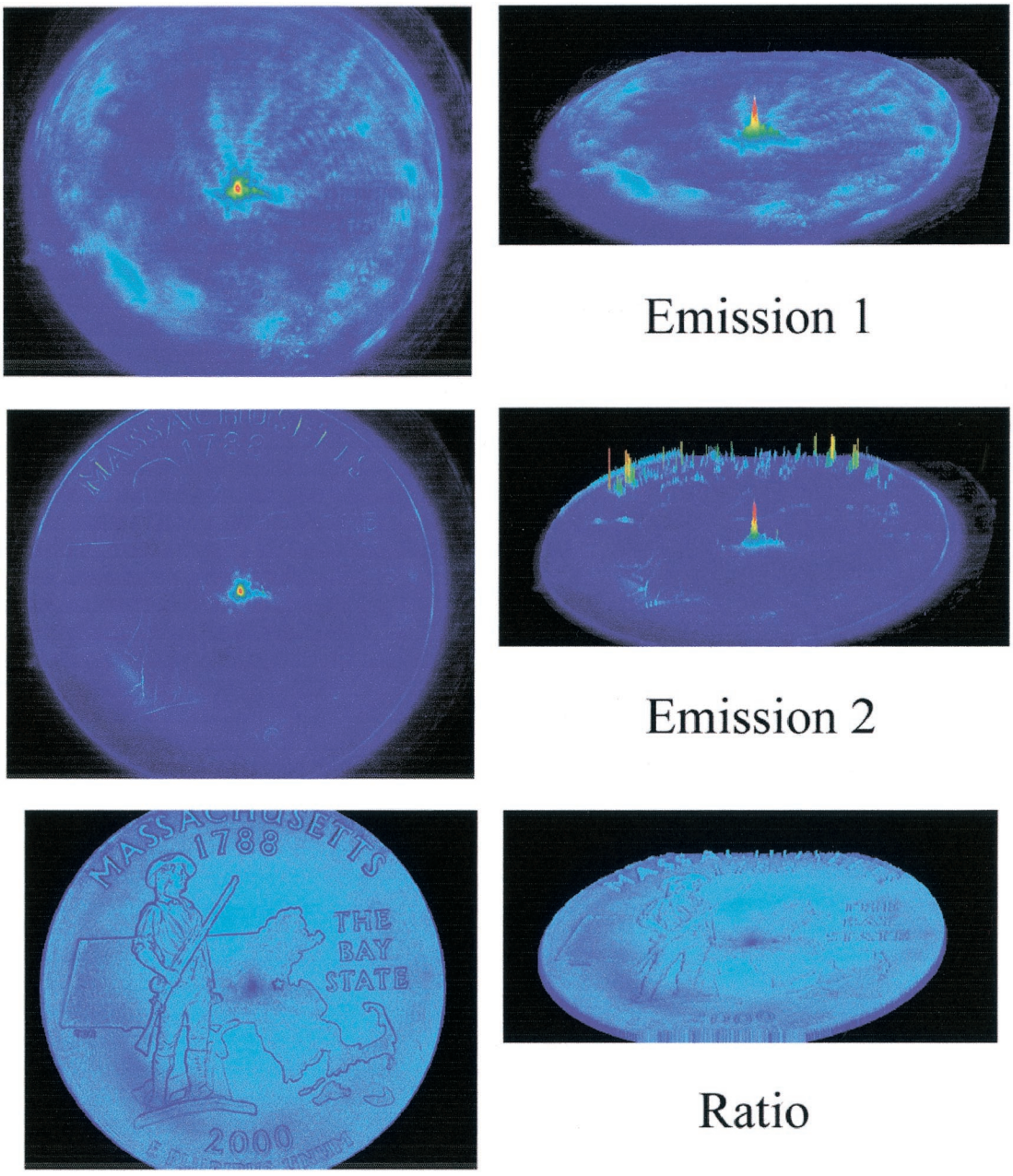

Fig. 1. Example of ERLIF.

coin surface features from fluorescent emission 1; nonetheless, this fluorescence provides a reasonable map of the laser beam's intensity profile. Some of the coin's features are apparent in fluorescent emission 2, but, again, fluctuations in the laser intensity profile prevent a clear interpretation of the coin's features from the basic laser-induced fluorescence signal. The bottom of Fig. 1 shows the ratio of the two fluorescence signals. The surface topography of the coin becomes evident—not simply as an image but as a quantifiable topography of the coin's surface. The clarity of this figure is evidence of the ability of this technique to eliminate local illumination variations while it preserves film-thickness information.

For ERLIF to properly suppress excitation intensity information in the ratio, the two fluorescent intensities must exhibit the same behavior with respect to excitation intensity. If the excitation photon flux is low, which is usually the case in continuous wave lasers, the fluorescent intensity is linearly proportional to the excitation intensity. Conversely, when the excitation photon flux is high, of the order of 10^{23}–10^{24} photons/s/cm^2 (approximately 37–370 MW/cm^2 at 532 nm) or higher, which is often the case when pulsed lasers are used, the fluorescent intensity is no longer linearly

proportional to the excitation intensity.[9,10] High excitation photon flux leads to nonlinear behavior of the fluorescent intensities with respect to the excitation intensity. If this behavior is not the same for the two fluorescent intensities, the ERLIF ratio will not suppress the dependence of fluorescence on excitation intensity. However, approximating the nonlinear behavior as a power law with respect to excitation intensity makes suppression of the excitation intensity still possible. This is accomplished through the use of a simple scheme that elevates the fluorescent intensity images to the appropriate exponents before ratioing. In this way, excitation intensity information in the ERLIF ratio is suppressed while film-thickness information is preserved.

In what follows, the principles and constitutive equations behind ERLIF film-thickness measurements are presented. The notation used in this paper is defined in Appendix A. A characterization of the fluorescence nonlinearity with excitation intensity is then introduced. This nonlinearity can introduce substantial differences in the excitation intensity behavior between the two fluorescent emissions of interested. If such differences do arise, suppression of excitation intensity in the ratio is no longer possible. It is then shown that a power law can be used to approximate the nonlinear behavior of the fluorescence over a finite excitation intensity range, letting fluorescent intensity be proportional to some power (less than unity) of the excitation intensity. On the basis of this approximation, a simple but powerful scheme is devised that permits preprocessing of the fluorescent intensity maps before the ratio operation is performed. It consists of elevating the two fluorescent intensities to appropriate exponents. In this manner it is possible to suppress the excitation intensity in the ratio even in the presence of different excitation intensity behaviors.

2. Emission Reabsorption Laser-Induced Fluorescence

ERLIF is a dual-fluorescence technique that permits accurate measurement of film thickness. This accuracy is achieved by suppression of excitation intensity information, allowing a direct and monotonic correlation to be made between fluorescent intensity and film thickness. Taking the ratio of the two fluorescent emissions cancels out the dependence of fluorescence on excitation intensity. Emission reabsorption of one fluorescent emission ensures that the dependences on thickness of the two fluorescent emissions are different and therefore do not cancel in the ratio. To appreciate the dynamics of the technique fully, one has to look at the equation that describes the total fluorescence signal collected by a photodetector (pixel in a CCD) as a function of film thickness. From the analysis of Hidrovo and Hart,[8]

$$E_f(t) = I_o \Phi A_f \tau_p \{1 - \exp[-\varepsilon(\lambda_{laser}) C t]\}. \quad (1)$$

We have neglected a monitoring efficiency factor in Eq. (1), which is a measure of what percentage of the total fluorescence signal (which is omnidirectional) is actually collected by the detector. Also, it has been assumed that the excitation and fluorescence intensities have a temporal square shape (square pulse) and that the duration of the fluorescence event is equal to the laser pulse width (τ_p), both reasonable assumptions. The time constant or, more correctly, the thickness constant for Eq. (1) is

$$t_c = 1/\varepsilon C. \quad (2)$$

This constant is the characteristic thickness scale of the fluorescence system and is a measure of the strength of the absorption process. The thickness constant determines the behavior of the fluorescent intensity with respect to film thickness. In most cases, the thickness constant encompasses only the absorption and resultant decrease of the exciting light's intensity as the light travels through a film of finite thickness. In other cases it is possible for the fluorescence itself to be absorbed by the film as it travels toward the detector (CCD) through the finite thickness. This phenomenon is known as emission reabsorption and depends primarily on the absorption and emission spectral characteristics of the fluorescent system.

In ERLIF two distinct fluorescent emissions are used: one that comprises emission reabsorption and another that lacks it. The two emissions are obtained by use of two dyes with appropriate spectral characteristics. Subscript 1 is used to represent the reabsorbed fluorescent emission and the spectral characteristics of the nonreabsorbing dye. Likewise, subscript 2 is used to represent the nonreabsorbed fluorescent emission and the spectral characteristics of the reabsorbing dye. The reabsorbed and nonreabsorbed fluorescent emissions are then given by[8]

$$E_{f,1}'(t, \lambda_{filter1}, y, \tau) = \frac{I_o(y, \tau)\varepsilon_1(\lambda_{laser}) C_1 \Phi_1(\lambda_{filter1}) A_f \tau_p (1 - \exp\{-[\varepsilon(\lambda_{laser}) C + \varepsilon_2(\lambda_{filter1}) C_2] t\})}{\varepsilon(\lambda_{laser}) C + \varepsilon_2(\lambda_{filter1}) C_2}, \quad (3)$$

$$E_{f,2}(t, \lambda_{filter2}, y, \tau) = \frac{I_o(y, \tau)\varepsilon_2(\lambda_{laser}) C_2 \Phi_2(\lambda_{filter2}) A_f \tau_p (1 - \exp\{-[\varepsilon(\lambda_{laser}) C] t\})}{\varepsilon(\lambda_{laser}) C}, \quad (4)$$

respectively. Two things should be noted from Eqs. (3) and (4): (1) the dependence of fluorescence onexcitation intensity is the same for both emissions (flu-

orescent intensity is linearly proportional to excitation intensity) and (2) because of reabsorption, the thickness constants of the two emissions are different. The thickness constants, which are given by

$$t_{c,1}' = \frac{1}{\varepsilon(\lambda_{\text{laser}})C + \varepsilon_2(\lambda_{\text{filter1}})C_2}, \tag{5}$$

$$t_{c,2} = \frac{1}{\varepsilon(\lambda_{\text{laser}})C}, \tag{6}$$

respectively, differ from each other in the term $\varepsilon_2(\lambda_{\text{filter1}})C_2$, which is the reabsorption term. As will become apparent presently, this difference in thickness constants between the two emissions is what permits preservation of the thickness information in the ratio.

Thus the ratio of the two fluorescent emissions is given by

$$R = \frac{E_{f,2}}{E_{f,1}'}, \tag{7}$$

$$R(t, \lambda_{\text{filter1}}, \lambda_{\text{filter2}}) = \frac{\varepsilon_2(\lambda_{\text{laser}})C_2\Phi_2(\lambda_{\text{filter2}})[\varepsilon(\lambda_{\text{laser}})C + \varepsilon_2(\lambda_{\text{filter1}})C_2](1 - \exp\{-[\varepsilon(\lambda_{\text{laser}})C]t\})}{\varepsilon_1(\lambda_{\text{laser}})C_1\Phi_1(\lambda_{\text{filter1}})\varepsilon(\lambda_{\text{laser}})C(1 - \exp\{-[\varepsilon(\lambda_{\text{laser}})C + \varepsilon_2(\lambda_{\text{filter1}})C_2]t\})}, \tag{8}$$

which is independent of excitation of intensity but still exhibits dependence on film thickness. Notice that this dependence on film thickness is embedded in the reabsorption term. If this term were zero, the one minus exponential terms of the two emissions would be identical and cancel in the ratio, making the ratio independent of film thickness.

In accordance with the previous research of Hidrovo and Hart,[8] an experimental system was set up to demonstrate the validity of the technique. The system consists of two CCD cameras mounted upon a single lens to record the two fluorescent emissions simultaneously. Dichroic mirrors and interference filters are used to separate and isolate the desired fluorescent emissions. Both mechanical and computer processing alignment of the two images is performed by means of adjustable optics and the use of a local cross-correlation algorithm.[11]

A calibration fixture was fabricated to provide a linearly increasing film thickness against which the technique could be tested. The fixture consisted of a quartz optical flat that formed the top and a quartz flat set at an angle with an inside reservoir channel etched around it (Fig. 2). When they were joined together, the optical flats produced a linearly increasing gap that was filled with liquid to produce a known film thickness. We measured the fixture by using a coordinate measuring machine to verify the thickness of the gap within the calibration area.

The two dyes selected to demonstrate the feasibility of the technique were Pyrromethene 567 and Pyrromethene 650. Both of these dyes are excitable by the 532-nm line of the frequency-doubled Nd:YAG laser used. As the technique was originally developed for lubrication and tribological purposes, the system was initially tested on its ability to measure oil films. The technique, however, can be used to measure almost any translucent substance that a dye can be mixed into or when there already exists a relatively broad-spectrum self-fluorescence characteristic when the dye is optically excited. A dye concentration of 8×10^{-4} mol/L of oil was used for both dyes. Figure 3 shows the dependence of fluorescence on film thickness for Pyrromethene 567 and Pyrromethene 650. There is a noticeable increase in fluorescence with film thickness that becomes nonlinear as the film thickness increases (optically thick system). It is apparent, however, that the laser intensity fluctuations are embedded within the film-thickness information, making it difficult to separate the two. The bottom of Fig. 3 shows the ratio of the two fluorescent emissions. Note the disappearance of the laser intensity fluctuations, illustrating that the laser intensity information is canceled in the ratio. Note also that the ratio has a nearly linear dependence on film thickness. As explained above, this is a consequence of reabsorption within the optically thick system.

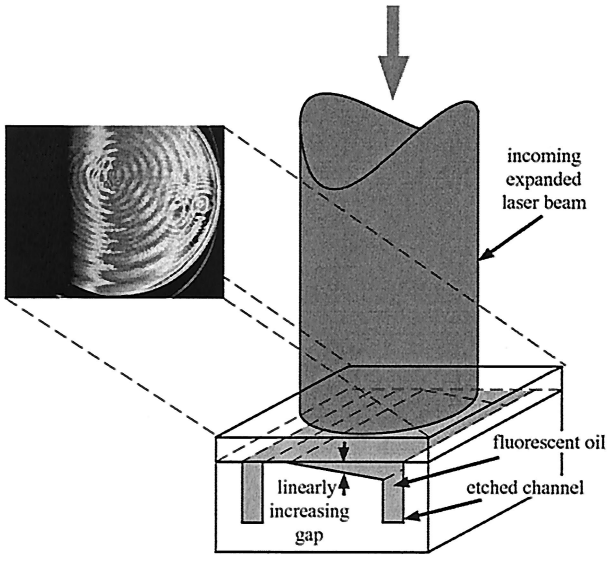

Fig. 2. Fixture and setup used for calibrating film thickness.

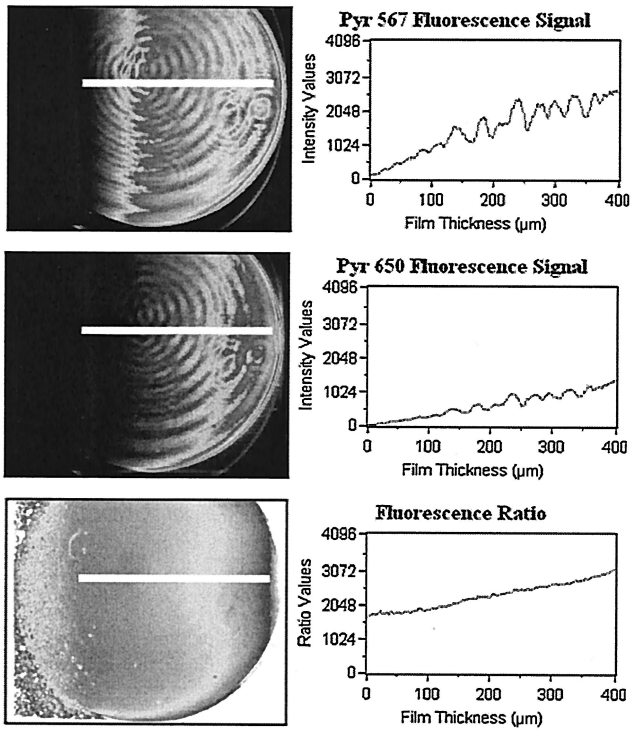

Fig. 3. Comparison of the film thickness laser-induced fluorescence signal for Pyrromethene 567 (Pyr 567) and Pyrromethene 650 (Pyr 650) versus their ratio (optically thick system with strong reabsorption).

3. Fluorescence Nonlinearity with Excitation Intensity

In the analysis of Hidrovo and Hart[8] and in Section 2 it was assumed that fluorescent intensity is directly proportional to or linear with excitation intensity. This is true (or partially true) only for low-excitation photon flux (intensity). Under high-excitation photon flux, of the order of 10^{23}–10^{24} photons/s/cm^2 (approximately 37–370 MW/cm^2 at 532 nm), depopulation of the ground state occurs as a consequence of the finite lifetime of the excited state. That is, the rate at which molecules are being excited is far greater than the rate at which they return to the ground state. This leads to an eventual saturation of the excited state and consequently of the fluorescent emission.

The basics of this behavior are presented by Yuzhakov *et al.*[9] and Patsayeva *et al.*[10] In their analysis it was shown that the time-dependent population of the excited state is given by

$$n_2(\tau) = \frac{nB\rho_o}{B\rho_o + A}\{1 - \exp[-(B\rho_o + A)\tau]\}, \quad 0 \le \tau \le \tau_p, \quad (9)$$

$$n_2(\tau) = \frac{nB\rho_o}{B\rho_o + A}[\exp(A\tau_p) - \exp(-B\rho_o\tau_p)]\exp(-A\tau), \quad \tau > \tau_p. \quad (10)$$

Equations (9) and (10) are based on the assumption of a square laser pulse in the temporal and spatial domains. This assumption is somewhat unrealistic in that most lasers used in fluorescence produce temporal and spatial pulses with Lorenzian, Gaussian, or similar shapes. However, it was shown by Georgiev *et al.*[12] that the influence of laser pulse shape on the fluorescence saturation condition is small for pulses with high peak intensity [greater than 10^{25} photons/s/cm^2] and short duration (less than 6 ns). Both of these conditions are met by the Nd:YAG laser system used for ERLIF purposes, whose average pulse intensity is of the order of 10^{25} photons/s/cm^2 (the peak intensity is therefore higher) and duration is 3 ns.

The fluorescence signal collected by the CCD is proportional to the total number of transitions from the excited state to the ground state and is given by

$$E_f = A_f \int_0^{\tau_e} I_f(\tau)\mathrm{d}\tau = \hbar\nu_{\mathrm{EM}} \int_0^{\tau_e} n_2(\tau)\mathrm{d}\tau. \quad (11)$$

As $\tau_e \to \infty$, which is appropriate for exposure times significantly longer than the laser pulse's duration plus the excited-state lifetime, integration of Eq. (11) with the proper substitution of Eqs. (9) and (10) yields

$$E_f = \frac{\hbar\nu_{\mathrm{EM}} nB\rho_o A_{21}}{(B\rho_o + A)}\left\{ \underbrace{\tau_p}_{\text{Term 1}} - \underbrace{\frac{1}{(B\rho_o + A)}}_{\text{Term 2}} + \underbrace{\frac{\exp[-(B\rho_o + A)\tau_p]}{(B\rho_o + A)}}_{\text{Term 3}} + \underbrace{\frac{1}{A}}_{\text{Term 4}} - \underbrace{\frac{\exp[-(B\rho_o + A)\tau_p]}{A}}_{\text{Term 5}} \right\}. \quad (12)$$

Equation (12) shows a nonlinear behavior of the fluorescence signal as a function of excitation photon flux (intensity). Looking at the extreme cases of low photon flux ($\rho_o \to 0$) and high photon flux ($\rho_o \to \infty$), we can show that

$$\lim E_f(\rho_o \to 0) = \frac{\hbar\nu_{\mathrm{EM}} nB\rho_o A_{21}\tau_p}{A}, \quad (13)$$

$$\lim E_f(\rho_o \to \infty) = \frac{\hbar\nu_{\mathrm{EM}} nA_{21}(A\tau_p + 1)}{A}, \quad (14)$$

denoting a signal that behaves quasi-proportionally to excitation intensity when low values are involved and tends to a constant saturated value for high excitation intensities.

Figure 4 shows a plot of Eq. (12) along with its decomposition into the terms within the braces (denoted Terms 1–5) as a function of excitation photon flux. The following dye and laser parameters (representative of the pyrromethene group and frequency doubled Nd:YAG) were used[12–14]: $B = \varepsilon/N_A = 2.4909 \times 10^{-17}$ cm^2, $A_{21} = 1/\tau_{21} = 1.667 \times 10^8$ s^{-1},

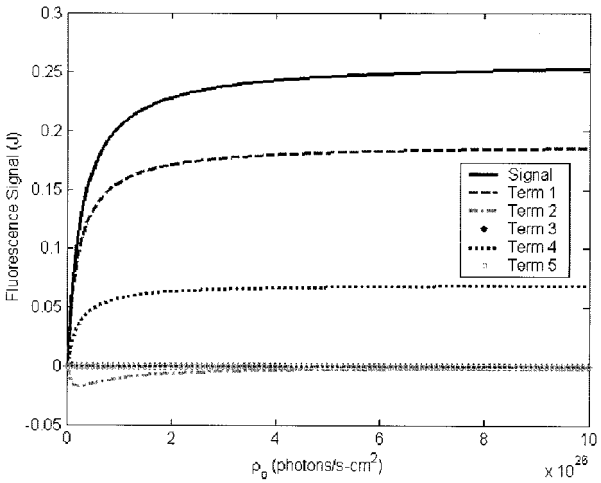

Fig. 4. Fluorescence signal as a function of excitation photon flux and its decomposition into various nonlinear terms.

$A = A_{21}/\Phi = 5.3763 \times 10^8\ \mathrm{s}^{-1}$, $\tau_p = 5 \times 10^{-9}$ s, and $\nu_{EM} = c/\lambda_{EM} = 4.8354 \times 10^{14}\ \mathrm{s}^{-1}$. In terms of the total number of dye molecules present, which is given by $n = CV = CA_f t$, a concentration of 2.4×10^{-2} mol/L, a fluorescence area of 4.9087 cm^2, and a film thickness of 50 μm, which correspond to conditions employed below in our experimental validation, give $n = 3.5473 \times 10^{17}$.

Although the behavior of the fluorescence signal with respect to excitation photon flux (intensity) is not obvious from Eq. (12), a look at Fig. 4 reveals that the signal's overall behavior is dominated by Terms 1 and 4. Thus we could characterize the behavior of the fluorescence signal with respect to excitation photon flux by defining a characteristic excitation photon flux (an excitation photon flux constant) in a way similar to what we did with Eqs. (1) and (2). This characteristic excitation photon flux is that photon flux that would make the terms in the denominator of the common factor of Eq. (12) of equal magnitude; thus

$$\rho_c = A/B. \tag{15}$$

This is the characteristic excitation photon flux of the fluorescence saturation behavior, a measure of when nonlinear effects become important. It makes sense that the characteristic excitation photon flux be given by Eq. (15), which implies equal activation and deactivation rates. For values much larger than ρ_c the activation rate is far greater than the deactivation rate and there exists a depopulation of the ground state with the consequent saturation of the excited state and corresponding fluorescent emission. For values much smaller than ρ_c, however, the activation rate is far less than the deactivation rate, such that the ground state is well supplied and the population of the excited state and corresponding fluorescence is dictated by excitation photon flux in a (quasi-) linear fashion.

At first glance, it appears that the fluorescence saturation behavior is independent of concentration (number of dye molecules). From Eq. (12) it can be seen that the fluorescence signal is directly proportional to n (and therefore to concentration). However, the analysis that led to Eq. (12) assumed an optically thin system with a constant excitation photon flux of ρ_o. If the thickness, the concentration, or both of the system are high enough, this assumption is not correct. For an optically thick system, the dependence of the excitation photon flux on depth must be taken into account. Equation (12) should then be rewritten to encompass only those molecules within an infinitesimal layer of the finite thickness of the system over which the excitation photon flux remains fairly constant: The situation is depicted in Fig. 5. Rewriting Eq. (12), we obtain

$$\mathrm{d}E_f = \frac{\hbar \nu_{EM} \mathrm{d}n B \rho_e A_{21}}{(B\rho_e + A)} \left\{ \tau_p - \frac{1}{(B\rho_e + A)} + \frac{\exp[-(B\rho_e + A)\tau_p]}{(B\rho_e + A)} + \frac{1}{A} - \frac{\exp[-(B\rho_e + A)\tau_p]}{A} \right\}, \tag{16}$$

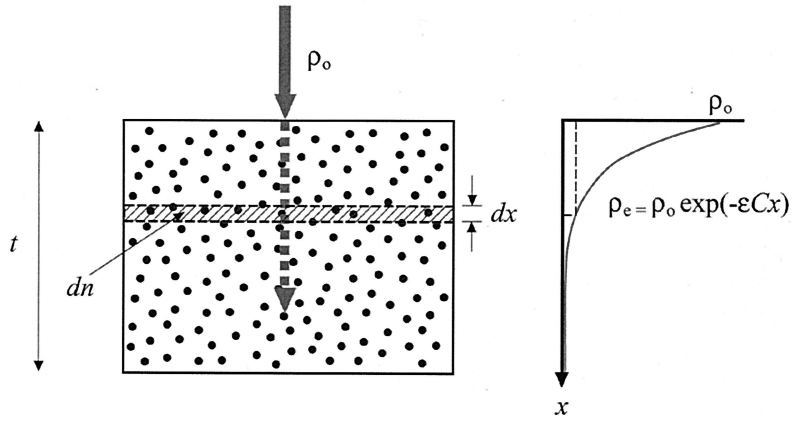

Fig. 5. Reduction of the excitation photon flux as a function of thickness owing to absorption (optically thick system).

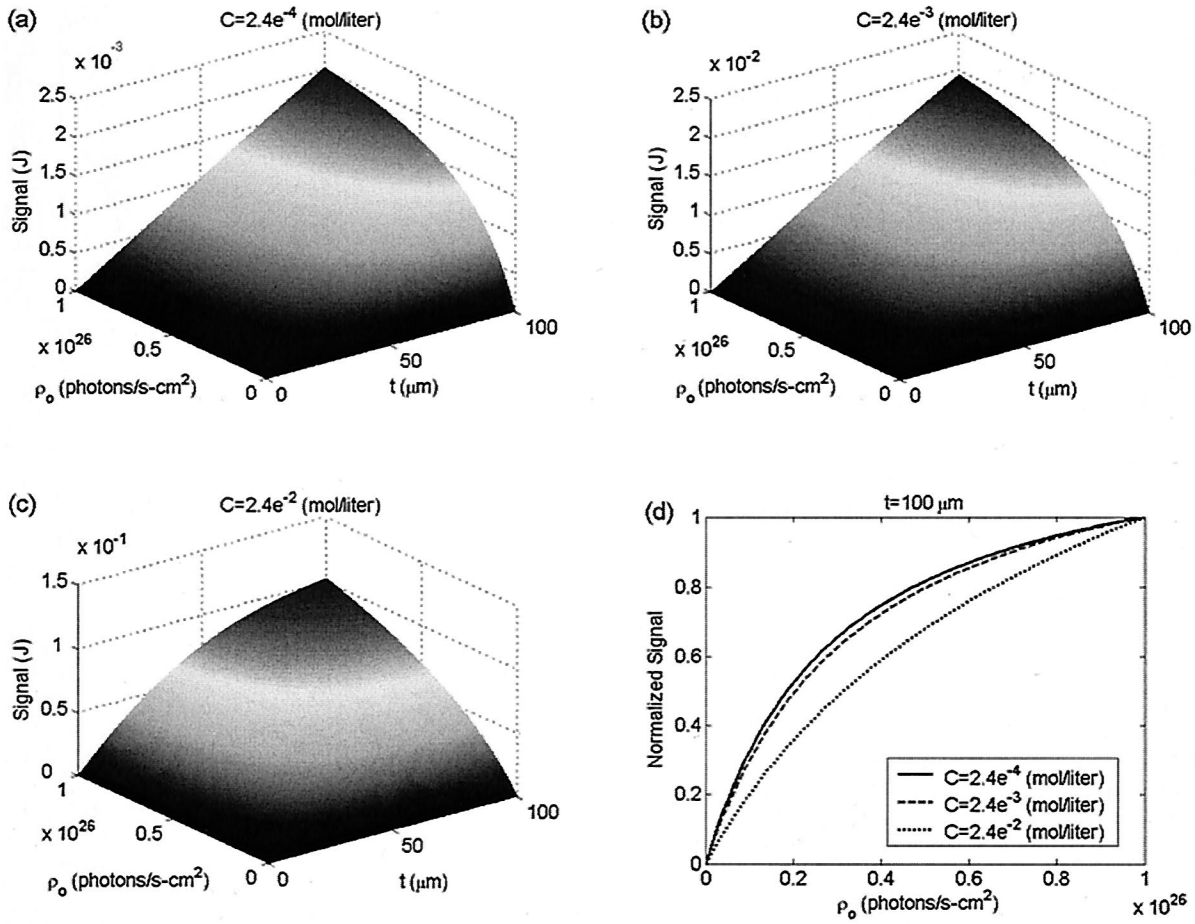

Fig. 6. (a)–(c) Fluorescence signals as a function of excitation photon flux and film thickness for three different dye molar concentrations C; (d) comparison of behavior of the signal as a function of ρ_o for the three concentrations (t = 100 μm).

and therefore

$$E_f = \int_0^t \mathrm{d}E_f, \tag{17}$$

where

$$\mathrm{d}n = CA_f N_A \mathrm{d}x \tag{18}$$

$$\rho_e = \rho_o \exp(-\varepsilon C x) = \rho_o \exp(-BN_A C x). \tag{19}$$

The total fluorescence signal is then obtained from the integration of Eq. (17) with proper substitution of Eqs. (18) and (19) into Eq. (16) over the finite thickness of the system (over all infinitesimal layers, to include all the molecules of the system). This integration cannot be solved analytically but rather must be solved numerically. Figures 6(a)–6(c) show the numerically obtained values of the total fluorescence signal (E) as a function of excitation photon flux (ρ_o) and film thickness (t) for three concentrations (C) that are orders of magnitude apart. Figure 6(d) shows the fluorescence signal (normalized to its maximum value) as a function of excitation photon flux for the three concentrations when the thickness of the system is 100 μm. It is apparent from Fig. 6 that the effects of concentration are more than just a mere amplification of the signal, especially under optically thick conditions. Under these conditions, concentration plays an important role in the behavior of fluorescence saturation with respect to excitation photon flux (intensity) behavior. Higher concentrations lead to a reduction of fluorescence saturation effects, as one can understand better by looking at Fig. 5.

If the system is optically thick, there is a substantial reduction of the excitation photon flux (intensity) as a function of thickness (depth). What this means is that, except for a few layers of molecules at the top, most layers embedded in the system will see a highly reduced excitation photon flux (intensity). The deeper one goes, the less change there is in this excitation photon flux as a function of thickness (depth). If the reduction is substantial enough to drive the value of ρ_e much below ρ_c (excitation photon flux constant), the fluorescence signal from the majority of the layers in the system (and therefore from the overall system) will approach the behavior given by Eq. (13). This occurs even though ρ_o (excitation photon flux at the surface of the system) is higher than ρ_c and a nonlinear behavior is expected. In optically thin systems,

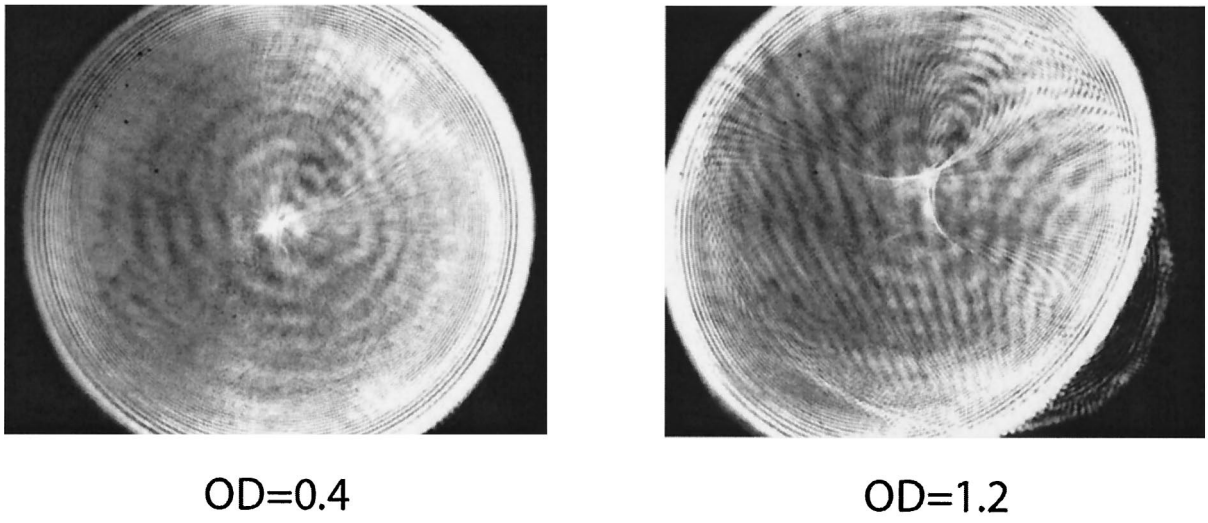

Fig. 7. Beam wander and distortion caused by aberrations in ND filters.

however, there is no substantial reduction of the excitation photon flux, and therefore the fluorescence saturation behavior is independent of C and depends only on ρ_o, as predicted by Eq. (12). See Fig. 6(d), in which the higher concentration exhibits a more nearly linear behavior with excitation photon flux than the lower concentrations show. Under the presumptions of Eq. (12), when they are normalized, all these curves should collapse into one.

4. Experimental Validation

As was mentioned above, the Nd:YAG laser that we used (New Wave Gemini PIV) is capable of producing excitation photon fluxes of the order of 10^{25} photons/s/cm^2 when the beam is expanded to a 2.5-cm diameter. This is more than enough intensity to introduce fluorescence saturation effects. Therefore we employed the same experimental setup that we used to demonstrate ERLIF for the fluorescence saturation experiments. The calibration fixture was filled with the oil–dye mixture to be probed, and the two-camera CCD system was used to record the fluorescent emissions. Although the CCD cameras provide information on the fluorescent emissions over a two-dimensional region, for our purposes here we used them as single photodetectors, averaging the signals from the pixels over the area of interest.

The laser was operated at full power settings. As the pulse-to-pulse energy stability of the laser is very good (maximum of 3.5% deviation), we used neutral-density (ND) filters to control the excitation photon flux. We employed four different ND filters, with optical densities (ODs) of 0.1, 0.2, 0.4, and 0.8. They effectively allowed us to use ODs that ranged from 0 to 1.5 in increments of 0.1 by stacking the filters. The only drawback with this method is that, because of manufacturing errors, the filters introduced nonuniform phase and amplitude transformations, which produced some wandering and distortion of the beam profile at the sample. For example, Fig. 7 shows the difference in beam profile and location at the sample for two ND filters combinations.

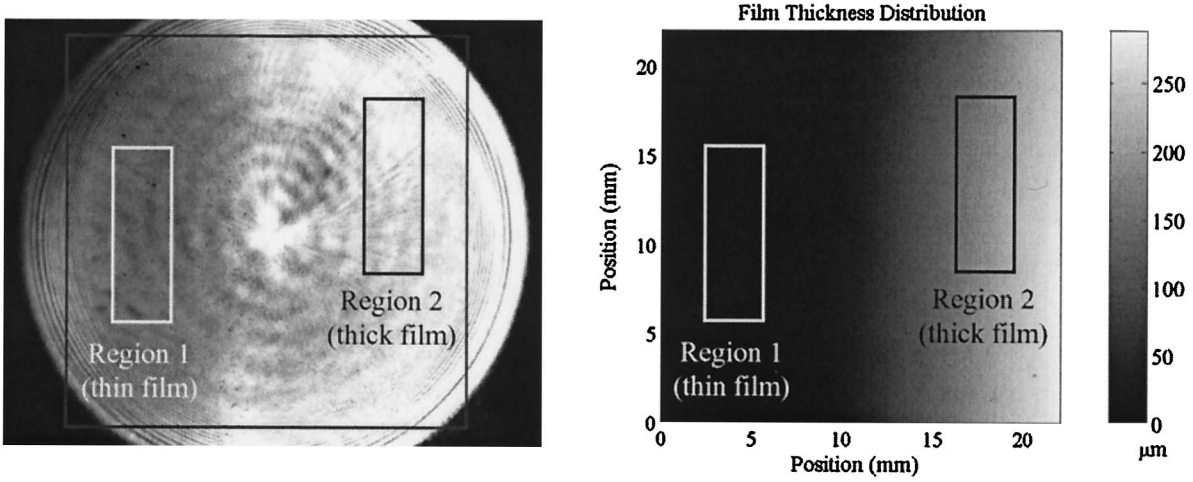

Fig. 8. Thin and thick film regions over which fluorescence signal measurements were taken and averaged.

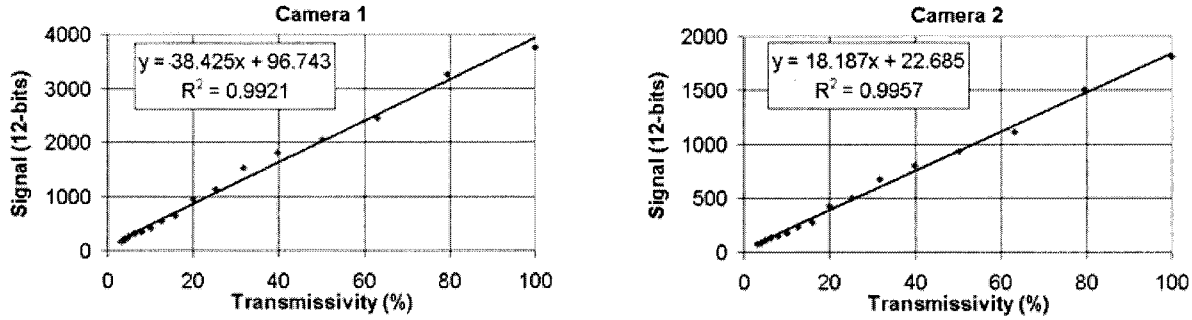

Fig. 9. Responses of imaging systems and characterization of ND filters.

Fluorescence signal measurements were taken over thin- (Region 1) and thick- (Region 2) film regions of the calibration fixture, as depicted in Fig. 8. The pixel values over these regions were averaged to yield the effective single photodetector signal. Before proceeding with the actual testing and data collection we made preliminary white-light measurements, using the ND filters, to ensure the linearity of the imaging system as a whole (camera plus optics). White light was shone onto a white diffusive surface (paper), and signal measurements were made with the ND filters placed in front of the imaging system. The results of this calibration are shown in Fig. 9, where the signals are plotted against the corresponding transmissivity of each ND filter combination. There is a small jitter in the expected linear behavior of these plots. The jitter is consistent between the two cameras and is therefore attributed mainly to discrepancies between the nominal and actual ODs of the ND filters and to the wander and distortion of the white-light profile introduced by them (as explained above).

Tests were conducted on nine oil–dye solutions. The dyes used were Pyrromethene 605 (P605) and Pyrromethene 650 (P650). We continue to use oil as a solvent because the ERLIF system was originally developed to measure lubricating films. Figure 10 shows the emission and absorption spectra of these dyes mixed in oil. The dye and the concentration used for each sample are listed in Table 1. Based on Table 1, the samples can be divided into three groups: P605 samples, P650 samples, and mixed P605 and P650 samples. For each group we used three concentrations, separated by an order of magnitude (factor of 10) and therefore termed low, medium, and high concentrations. Note that the concentrations were kept consistent between the single- and mixed-dye samples. The relative concentrations of P605 and P650 were chosen based on the mixed-dye, high-concentration sample, which was tailored (as explained by Hidrovo and Hart[8]) toward the measurement of thin films of the order of 10 μm with a resolution of 1 μm.

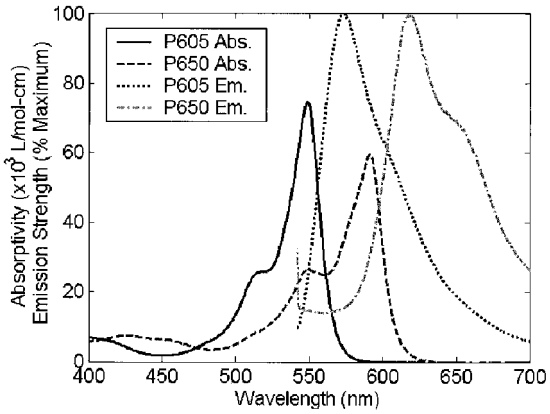

Fig. 10. Emission (Em.) and absorption (Abs.) spectra for Pyrromethene 605 (P605) and Pyrromethene 650 (P650).

The imaging systems (cameras) were synchronized to the laser, which was operated in manual single-shot mode. The exposure times of the cameras were set at 1 ms, short enough to reduce unwanted stray light and background signal but long enough to capture the short fluorescent event in its totality. The appropriate ND filter combinations were placed at the exit of the laser beam expander to control the excitation intensity hitting the sample, going from full intensity of the order of 10^{25}–10^{26} (photons/s)cm^2] to ~3% of full intensity (OD, 1.5). For each filter combination (OD), ten measurements were made and their average value used as a data point. To account for possible photobleaching effects, this progression was repeated backward, going now from ~3% of full intensity (OD, 1.5) to full intensity. Thus there would be two data points for each OD value. For each sample we looked at the fluorescence signals at 580 nm (camera 1) and 620 nm (camera 2) from the thin- (Region 1) and thick- (Region 2) film regions. The results of the tests are shown in Figs. 11–14. Each figure encompasses data for the three sample groups mentioned above (single P605, single P650, and mixed P605 and P650 samples) and concentrations (low, medium, and high) at a given wavelength/camera (580 nm/camera 1 or 620 nm/camera 2) pair and for a given region (Region 1 or Region 2). At the left in these figures the raw fluorescence signal is plotted against excitation intensity, whereas, at the right, each data curve is normalized relative to its maximum signal to facilitate a comparison of the nonlinear behavior of the various concentrations.

In all cases the fluorescence signal exhibits some

Table 1. Dyes and Concentrations Employed in the Samples Tested

Sample (Description)	Dye	Concentration (mol/L)
1 (single P605, low)	Pyrromethene 605	8×10^{-5}
2 (single P605, medium)	Pyrromethene 605	8×10^{-4}
3 (single P605, high)	Pyrromethene 605	8×10^{-3}
4 (single P650, low)	Pyrromethene 650	2.4×10^{-4}
5 (single P650, medium)	Pyrromethene 650	2.4×10^{-3}
6 (single P650, high)	Pyrromethene 650	2.4×10^{-2}
7 (mixed, low)	Pyrromethene 605–Pyrromethene 650	8×10^{-5} 2.4×10^{-4}
8 (mixed, medium)	Pyrromethene 605–Pyrromethene 650	8×10^{-4} 2.4×10^{-3}
9 (mixed, high)	Pyrromethene 605–Pyrromethene 650	8×10^{-3} 2.4×10^{-2}

degree of nonlinearity with respect to excitation intensity (photon flux). The most linear behavior is exhibited by the signals of the samples of mixed dyes at high concentrations [Figs. 11(f), 12(f), 13(f), and 14(f)], which have the highest net effective concentration (P605 concentration plus P650 concentration). This result is in agreement with the theoretical analysis made in Section 3, where it was shown that concentration and optical thickness lessen the nonlinear behavior of the fluorescence signal [Fig. 6(d)]. The influence of optical thickness on this effect can also be appreciated (though to a lesser extent) if one compares the signals from the single P650 at high concentration in the thin- (Region 1) and thick- (Region 2) film regions. The signals from the thick-film regions [Figs. 12(d) and 14(d)] behave slightly more linearly than their thin-film region counterparts [Figs. 11(d) and 13(d)]. The signals from the single P605 group (low, medium, and high concentration samples), however, which have the lowest concentrations in relation to the other groups, exhibit optically thin behavior. Under these conditions the nonlinear behavior is independent of concentration, and all the curves collapse into one when they are normalized, as can be seen from Figs. 11(b), 13(b) and 14(b) [but not in Fig. 12(b) because of saturation of the camera rather than of the fluorescent signal, but similar behavior is expected]. This result is also in agreement with the theoretical analysis of Section 3, where it was shown that for optically thin systems, for which the excitation photon flux is essentially constant throughout the sample depth, Eq. (12) is readily applicable. Under conditions of Eq. (12), the role of the concentration (number of molecules, n) is that of amplification or gain of the fluorescence signal with no influence on the signal's nonlinear behavior relative to excitation photon flux.

Of particular interest is the behavior of signals at 620 nm (camera 2) for the medium concentration samples containing P650 (mixed dyes and single P650). These medium concentration signals exhibit a more nearly nonlinear behavior than their low and high concentration counterparts [Figs. 13(d), 13(f), 14(d), and 14(f)]. From the theoretical analysis of Section 3 and as was pointed out above, one would have expected these medium concentration signals to lie in between the low and high concentrations signals, exhibiting an intermediate behavior (more nearly nonlinear than the high but less than the low), just as depicted in Fig. 6(d). We attribute this unusual and unexpected behavior to concentration-dependent fluorescence quenching[15,16] of P650 molecules.

Certain fluorophores tend to quench each other when they are in very close proximity (a few nanometers) to one another.[17] Although the specifics of this quenching process can be quite involved (formation of a triplet state, for example), the net effect of quenching is to reduce the spontaneous-emission rate constant (A_{21}), which in turns means a reduction in the total transition rate from the excited state to the ground state ($A = A_{21} + A_{21}'$). From Eq. (15), a reduction in A implies a lower excitation photon flux constant ρ_c and, therefore, appearance of nonlinear behavior at lower intensities (depicted as more-severe nonlinear behavior over a given range of intensities). The nonlinear behavior is less, and there is a return to more nearly linear behavior when the concentration is increased further [high concentration samples; Figs. 13(d), 13(f), 14(d), and 14(f)]. The reason for this is twofold: (1) Further increasing the concentration pushes the system into the optically thick regime with the consequent linearization of the behavior as a result of excitation photon flux absorption (see Section 3) and, more importantly, (2) the proximity of the fluorophore can also lead to shorter excited-state lifetimes ($\tau_L = 1/A$) because of the shorter nonradiative lifetime of the excited state ($\tau_{21}' = 1/A_{21}'$), leading to an increase in A_{21}' and, therefore, causing A to counteract the effects of the decrease of A_{21}.[18]

The concentration quenching of the fluorescence signal for the medium concentration samples is evident when one looks at the raw fluorescence signal in Region 1 [thin film; Figs. 13(c) and 13(e)]. In this region, where fluorescence reabsorption effects are not so substantial, the gain signal achieved in going from the low to the medium concentration is not so substantial as the gain achieved in going

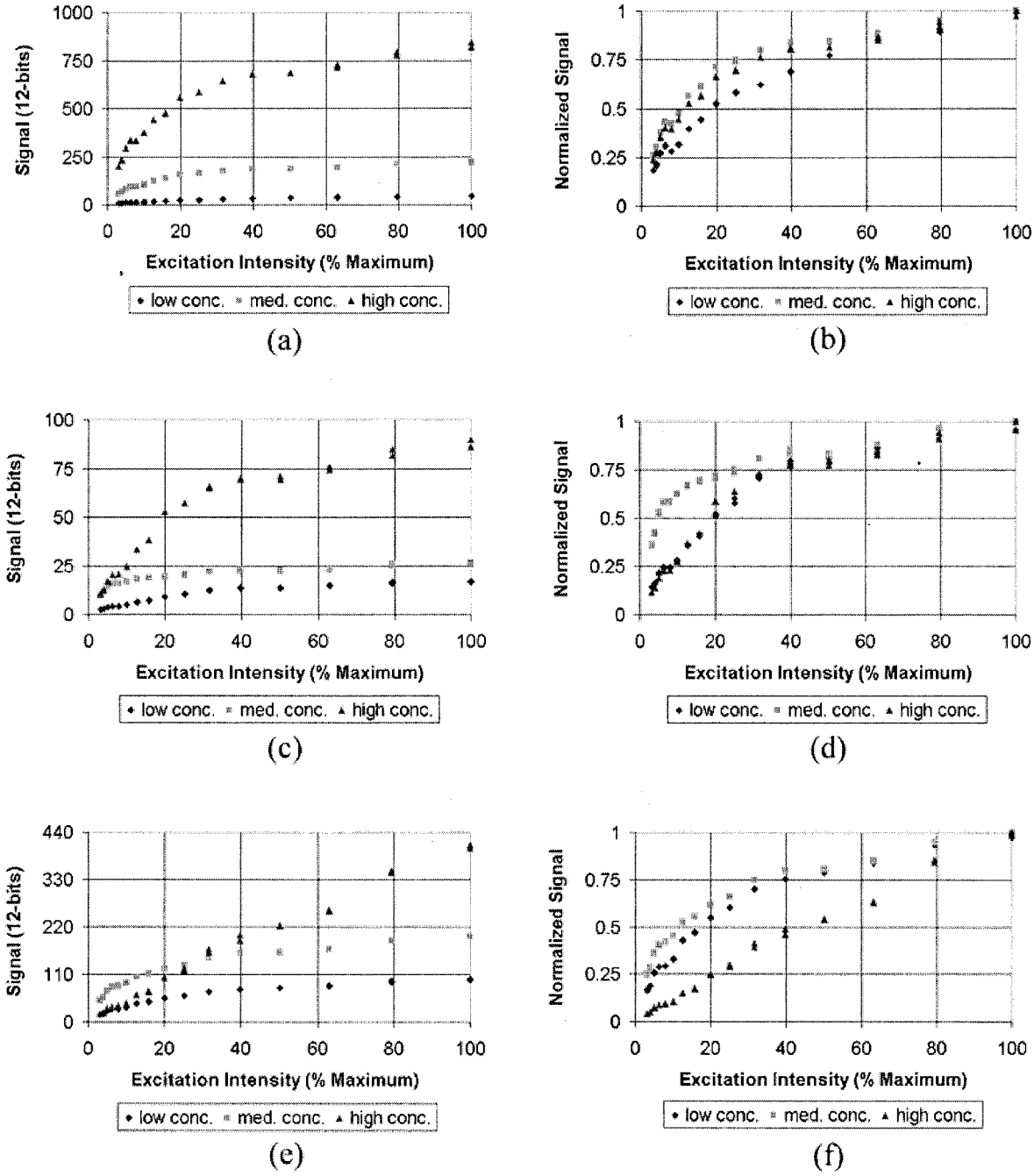

Fig. 11. Results of tests for camera 1 (580 nm), Region 1 (thin film thickness): (a) single P605, (b) single P605 normalized, (c) single P650, (d) single P650 normalized, (e) mixed P605/P650, (f) mixed P605/P650 normalized.

from the medium to the high concentration, even though the jumps in concentration are equivalent (an order of magnitude apart). We believe that this concentration-quenching-induced behavior (medium concentration more nearly nonlinear than low and high concentrations) is characteristic only of P650 because the single P605 samples do not exhibit this behavior. Furthermore, in the mixed-dye samples, only the 620-nm signals (camera 2) show this behavior [Figs. 13(f) and 14(f)], whereas the 580-nm signals (camera 1) do not [Figs. 11(f) and 12(f)]. This result is in accordance with the fact that, in the mixed-dye samples, the 620-nm signal comes mainly from P650 fluorescence, whereas the same is true for the 580-nm signal and P605 fluorescence.

Although the raw fluorescence signal plots (at the left in Figs. 11–14) do not provide much insight into the relative nonlinear behavior, they do provide information about the relative strength of the signals. The trends observed with regard to this relationship can be accounted for by the analysis behind ERLIF

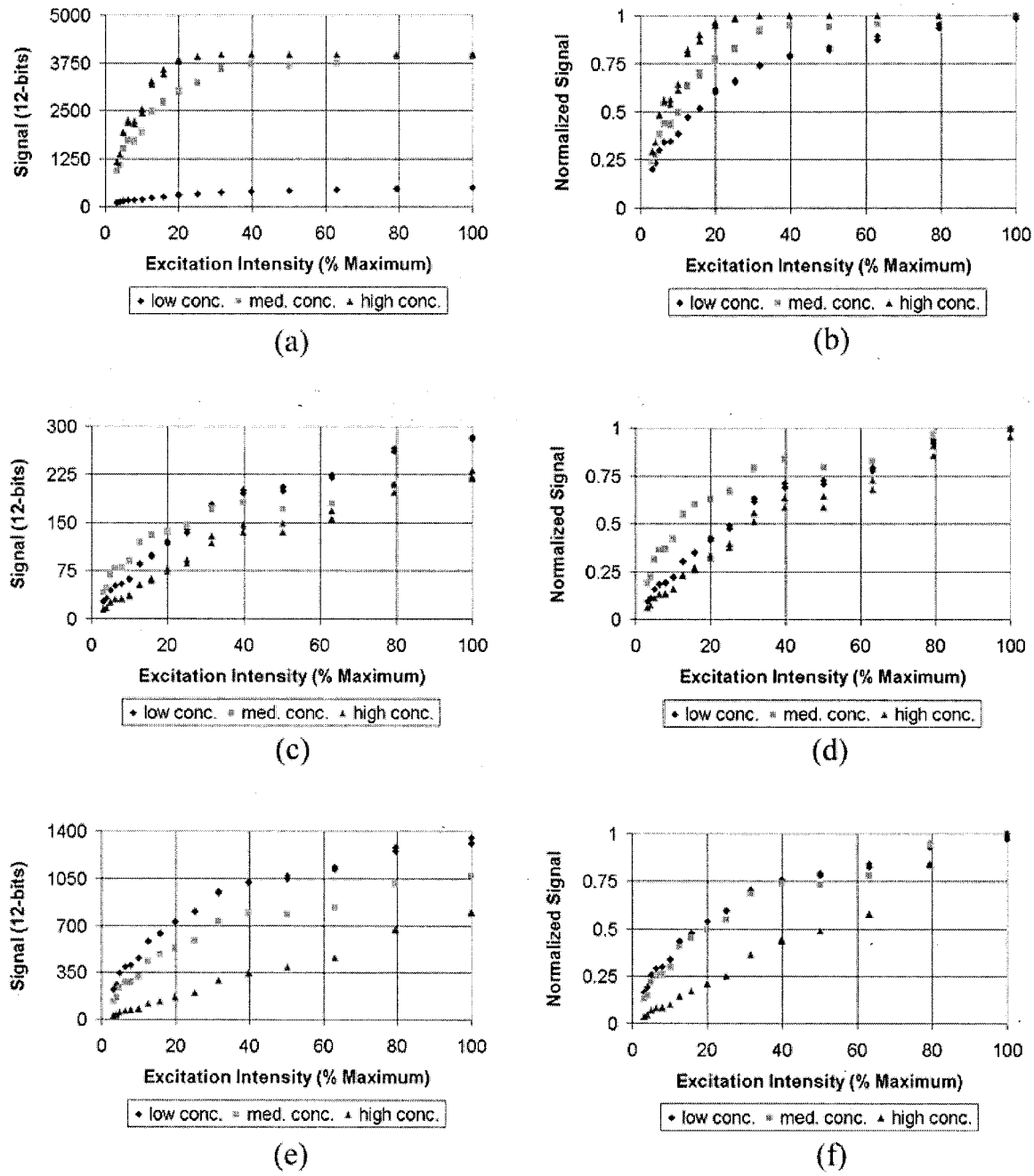

Fig. 12. Results of tests for camera 1 (580 nm), Region 2 (thick film thickness): (a) single P605, (b) single P605 normalized, (c) single P650, (d) single P650 normalized, (e) mixed P605/P650, (f) mixed P605/P650 normalized.

characterization. The signals from the single P605 samples behave in the manner that one would expect, with the intensity of the signal increasing with concentration. With the introduction of P650 (mixed-dye and single P650 samples), this is not necessarily the case in some instances when the previous behavior is completely reversed [Fig. 12(e)]. This contradictory behavior (inverse relationship between signal and concentration) is due to reabsorption effects introduced by the presence of P650. Thus, even though the concentration of the dye that produces the signal at 580 nm is increasing, so is the concentration of P650 (reabsorbing dye), which quenches the fluorescence signal. Reabsorption is most noticeable for the 580-nm signals because there is a substantial overlap of the P650 absorption spectrum for this emission (Fig. 10) and for Region 2 where the system is optically thicker. Thus the 620-nm signals of Region 1 do not show this behavior and still adhere to the conventional signal gain with concentration [Figs. 13(c) and 13(e)]. On the other hand the 580-nm signals of Region 2 exhibit a complete behavior reversal [Figs. 12(c) and 12(e)].

In Region 1 the conditions are not optically thick

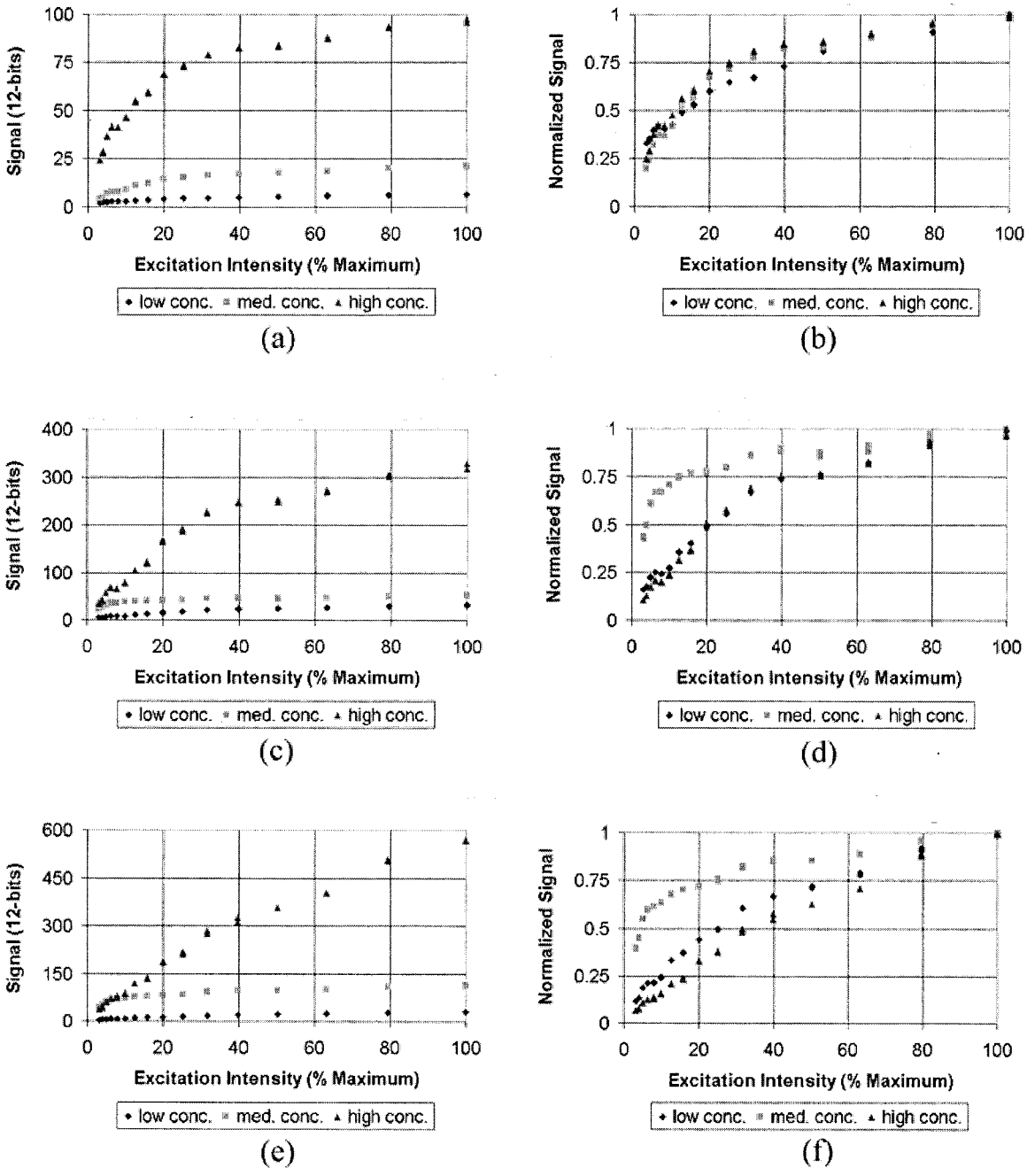

Fig. 13. Results of tests for camera 2 (620 nm), Region 1 (thin film thickness): (a) single P605, (b) single P605 normalized, (c) single P650, (d) single P650 normalized, (e) mixed P605/P650, (f) mixed P605/P650 normalized.

enough, and the effects of reabsorption can be observed only for low excitation intensities, even for the 580-nm signals [Figs. 11(c) and 11(e)]. More interesting still is the fact that, even for the 620-nm signal under optically thick conditions (Region 2), the effects of reabsorption can be observed [Figs. 14(c) and 14(e)]. In these instances, the high concentration signals lie between the low and the medium concentration signals. From Fig. 10 it is apparent that at the 620-nm emission there is still a small overlap with the P650 absorption spectrum. This overlap, albeit small, is enough to introduce reabsorption effects when the highest P650 concentration is used.

5. Excitation Nonlinearity in ERLIF: The Power Law Approximation

The core of the ratiometric approach to suppression of excitation intensity information relies on the assumption that both fluorescent intensities are linearly proportional to the excitation intensity. As was seen above and in the analysis of Hidrovo and Hart,[8] this leads to cancellation of the fluorescent intensity information in the ratio of Eq. (8). This result presupposes that the mean intensity of the excitation source and its fluctuations (in both space and time) are small. However, as we have seen in

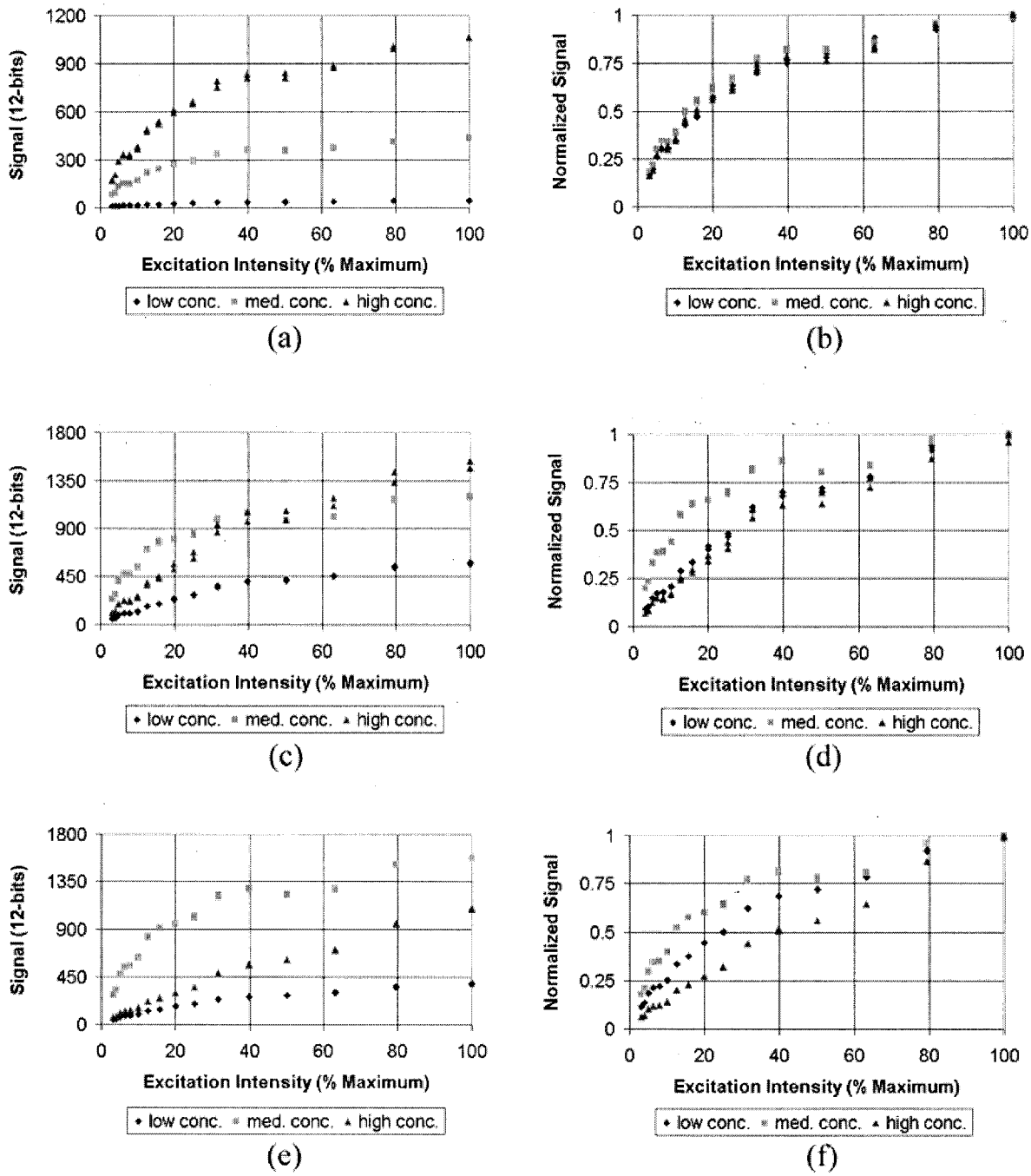

Fig. 14. Results of tests for camera 2 (620 nm), Region 2 (thick film thickness): (a) single P605, (b) single P605 normalized, (c) single P650, (d) single P650 normalized, (e) mixed P605/P650, (f) mixed P605/P650 normalized.

Sections 3 and 4, when high-energy laser pulses are used, such is not the case, and the fluorescence signal behaves in a nonlinear manner with respect to excitation intensity. This nonlinear behavior could constitute a challenge for the proper suppression of excitation intensity by the ratiometric approach.

At first glance it would appear that nonlinear behavior of the fluorescence with excitation intensity would forbid suppression of the excitation intensity in a ratiometric approach. It turns out that it does not matter what type of dependence the fluorescent intensity has on the excitation intensity. The dual fluorescence ratiometric approach still suppresses information on excitation intensity as long as the two fluorescent intensities have the same dependence on excitation intensity. To illustrate this, we write the fluorescent intensities as the product of two functions: one containing the dependence of fluorescence on excitation intensity and the other containing all the remaining dependences:

$$E_{f,1}' = F_1(I_e)G_1(\varepsilon, C, t\ldots), \tag{20}$$

$$E_{f,2} = F_2(I_e)G_2(\varepsilon, C, t\ldots). \tag{21}$$

Taking the ratio of the two fluorescent emissions yields

$$R = \frac{E_{f,2}}{E_{f,1}'} = \frac{F_2(I_e)G_2(\varepsilon, C, t\ldots)}{F_1(I_e)G_1(\varepsilon, C, t\ldots)}. \tag{22}$$

If $F_1(I_e) = F_2(I_e)$,

$$R = \frac{E_{f,2}}{E_{f,1}'} = \frac{G_2(\varepsilon, C, t\ldots)}{G_1(\varepsilon, C, t\ldots)} \tag{23}$$

and the fluorescence ratio is equally independent of excitation intensity. However, if $F_1(I_e) \neq F_2(I_e)$, then

$$R = \frac{E_{f,2}}{E_{f,1}'} = \frac{F_2(I_e)G_2(\varepsilon, C, t\ldots)}{F_1(I_e)G_1(\varepsilon, C, t\ldots)} = F_R(I_e)\frac{G_2(\varepsilon, C, t\ldots)}{G_1(\varepsilon, C, t\ldots)}, \tag{24}$$

and the ratio itself has a dependence on excitation intensity, $F_R(I_e)$, as illustrated in Fig. 15, which shows the ERLIF fluorescence and ratio images for the thin gap (thin-film thickness) region of the calibration fixture. In this instance, high-resolution small-film thickness measurements (less than 20 μm) are desired. The fluorescent dyes used for these purposes were P605 and P650 at concentrations of 8×10^{-3} mol/L of oil and 2.4×10^{-2} mol/L of oil, respectively. The small-film thickness measurements required high fluorescence efficiency dyes and much higher concentrations than those used in the experiments described by Hidrovo and Hart.[8] From the top and middle images of Fig. 15 it can be seen that the fluorescence images portray, as expected, the fluctuations in laser spatial intensity. This is a consequence of the dependence of fluorescence on excitation intensity as predicted by Eq. (1). It is also apparent from the bottom image of Fig. 15 that the laser's spatial intensity fluctuations are still markedly present in the ratio image. Consequently, this ratio image still has some functionality with respect to laser intensity as prescribed by Eq. (24), which indicates that the dependences of fluorescent emissions on excitation intensities are different from each other.

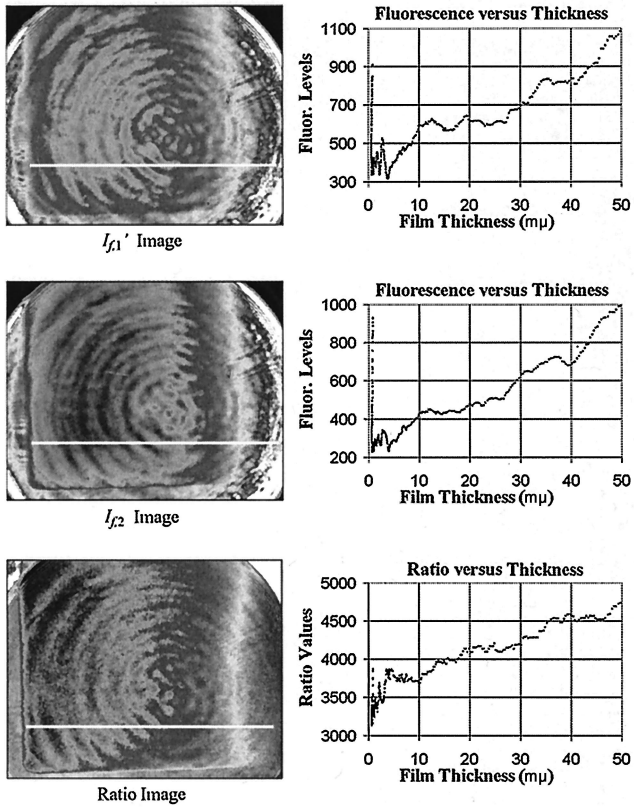

Fig. 15. Fluorescence and ERLIF ratio images for thin-film thickness.

To implement a practical approach that would permit suppression of the excitation intensity in the ratio when the dependences of the fluorescent emissions on excitation intensity are different from each other (more on this in Section 6), we propose to approximate the nonlinear excitation intensity dependence by a power law of the form

$$E_f \propto I_e^{\gamma}, \tag{25}$$

where $\gamma \leq 1$ ($\gamma = 1$ corresponds to a linear dependence. We refer to γ as the nonlinear power exponent). Thus, after appropriate substitutions, for the total fluorescence signal of dye 1 (reabsorbed dye) we have

$$E_{f,1}'(t, \lambda_{\text{filter1}}, y, \tau) = \frac{I_o(y, \tau)^{\gamma_1}\varepsilon_1(\lambda_{\text{laser}})C_1\Phi_1(\lambda_{\text{filter1}})A_f\tau_p(1 - \exp\{-[\gamma_1\varepsilon(\lambda_{\text{laser}})C + \varepsilon_2(\lambda_{\text{filter1}})C_2]t\})}{\gamma_1\varepsilon(\lambda_{\text{laser}})C + \varepsilon_2(\lambda_{\text{filter1}})C_2}, \tag{26}$$

and, for the total fluorescence signal of dye 2,

$$E_{f,2}(t, \lambda_{\text{filter2}}, y, \tau) = \frac{I_o(y, \tau)^{\gamma_2}\varepsilon_2(\lambda_{\text{laser}})C_2\Phi_2(\lambda_{\text{filter2}})A_f\tau_p(1 - \exp\{-[\gamma_2\varepsilon(\lambda_{\text{laser}})C]t\})}{\gamma_2\varepsilon(\lambda_{\text{laser}})C}. \tag{27}$$

This dependence of fluorescence on excitation intensity can approximate the actual nonlinear behavior, albeit only over a finite excitation intensity region. Which region that will be will depend on the value of γ. Figure 16 shows comparisons of the actual fluores-

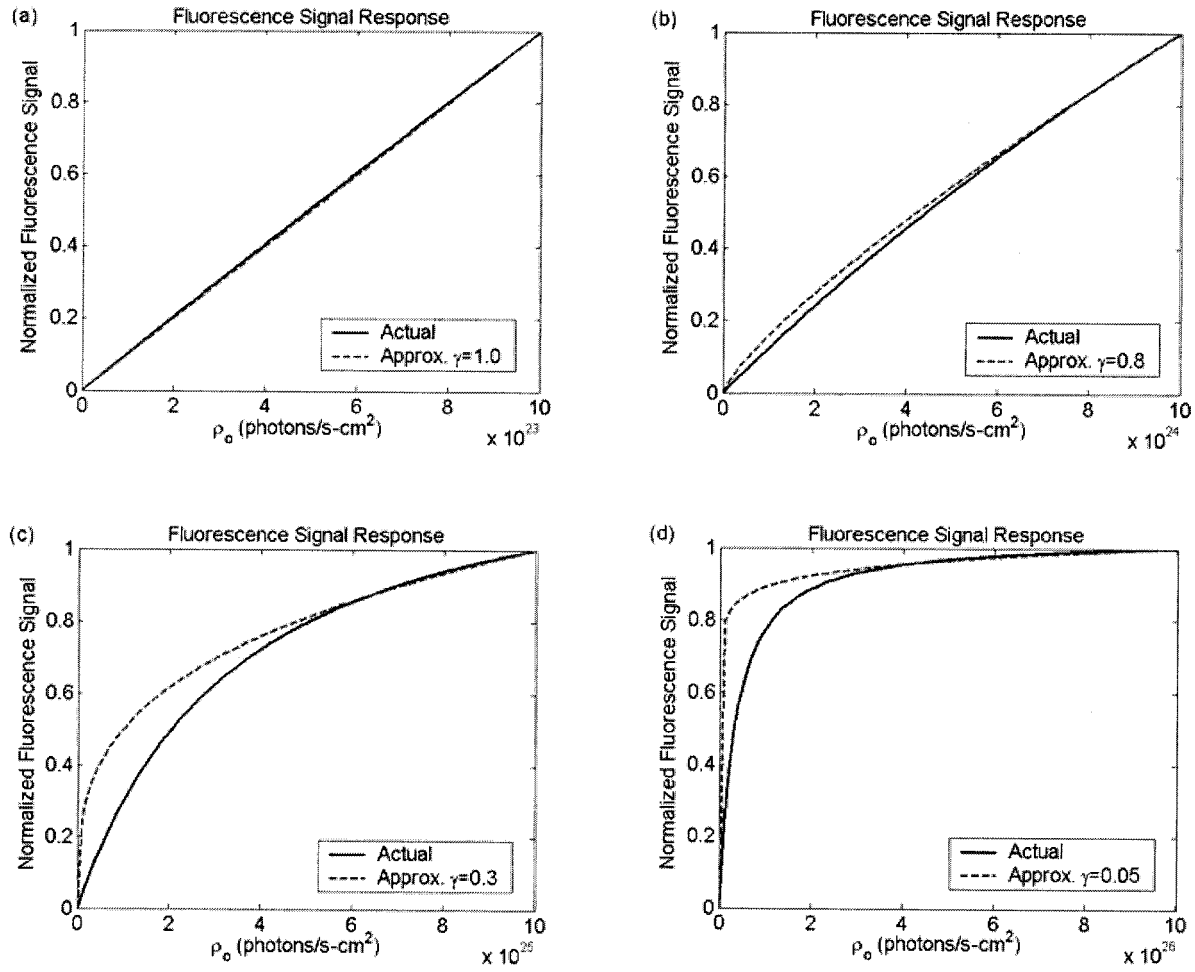

Fig. 16. Comparison of actual and approximate (power law) fluorescence behavior with excitation intensity for several values of ρ_o and γ.

cence signal as a function of excitation photon flux [numerical integration of Eq. (17)] and the power law approximation [Eq. (26) or (27); their functionality with respect to excitation intensity is the same] for several ranges of photon excitation fluxes and values of γ. It is apparent from Fig. 16 that changing the value of γ allows for different regions of the nonlinear curve to be approximated by the power law. As the range of excitation intensities increases and the fluorescence behavior becomes more nearly nonlinear, tending toward saturation, the optimum value of γ decreases. Note that, for low excitation photon fluxes, the optimum value of γ is 1 [Fig. 16(a)], which indicates a behavior that is almost linear (or tends to linearity), as one would expect from Eq. (13). Although these comparisons are specific to a given set of parameters that are representative of the pyrromethene dye group, nonlinear behavior of the fluorescent intensity with respect to excitation photon flux is characteristic of most fluorophores, and the power law approximation would still apply.

6. Power Law Approximation Processing Scheme

The power law approximation of fluorescence relative to excitation intensity leads to a simple scheme that is capable of neutralizing the dependence of the ratio on excitation intensity.[19] As mentioned above, it does not matter that the fluorescence behavior with respect to excitation intensity is nonlinear as long as the two fluorescent emissions have the same type of nonlinear dependence on excitation intensity. Even if the nonlinear behaviors of the two fluorescent emissions are not the same, it is possible to apply the power law approximation and minimize the effect of any difference in linearity. Thus, if

$$E_{f,1}' \propto I_o^{\gamma_1}, \tag{28}$$

$$E_{f,2} \propto I_o^{\gamma_2}, \tag{29}$$

as in Eqs. (26) and (27), and we let

$$\Gamma = \gamma_1/\gamma_2, \tag{30}$$

then

$$R = E_{f,2}^{\Gamma}/E_{f,1}' \tag{31}$$

is no longer a function of I_o, as

$$E_{f,2}^{\Gamma} \propto (I_o^{\gamma_2})^{\Gamma} = (I_o^{\gamma_2})^{\gamma_1/\gamma_2} = I_o^{\gamma_1}, \tag{32}$$

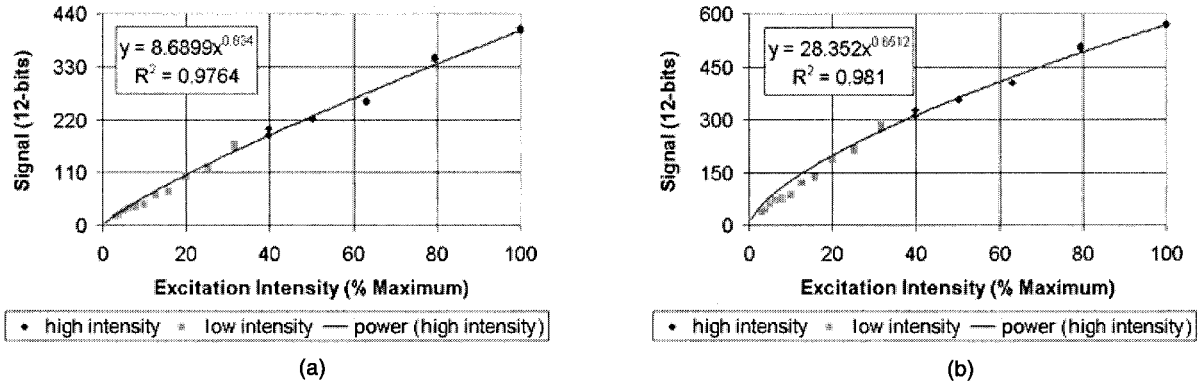

Fig. 17. Fluorescence signal as a function of excitation intensity and power law regression fitting for high concentration mixed-dye samples in Region 1 (thin film): (a) 580 nm (Camera 1) signal with power regression fit $\gamma_1 = 0.834$ and (b) 620 nm (Camera 2) signal with power regression fit $\gamma_2 = 0.6512$.

which has the same dependence on I_o that $E_{f,1}'$ has. Expanding the whole of relation (32), we obtain

$$E_{f,2}(t, \lambda_{\text{filter1}}, y, \tau)^{\Gamma} = \frac{I_o(y, \tau)^{\gamma_1}[\varepsilon_2(\lambda_{\text{laser}})C_2\Phi_2(\lambda_{\text{filter2}})A_f\tau_p]^{\Gamma}(1 - \exp\{-[\gamma_2\varepsilon(\lambda_{\text{laser}})C]t\})^{\Gamma}}{[\gamma_2\varepsilon(\lambda_{\text{laser}})C]^{\Gamma}}, \tag{33}$$

such that

$$R = \frac{E_{f,2}{}^{\Gamma}}{E_{f,1}{}'}, \tag{34}$$

$$R(t, \lambda_{\text{filter1}}, \lambda_{\text{filter2}}) = \frac{(A_f\tau_p)^{\Gamma-1}[\varepsilon_2(\lambda_{\text{laser}})C_2\Phi_2(\lambda_{\text{filter2}})]^{\Gamma}[\gamma_1\varepsilon(\lambda_{\text{laser}})C + \varepsilon_2(\lambda_{\text{filter1}})C_2](1 - \exp\{-[\gamma_2\varepsilon(\lambda_{\text{laser}})C]t\})^{\Gamma}}{\varepsilon_1(\lambda_{\text{laser}})C_1\Phi_1(\lambda_{\text{filter1}})[\gamma_2\varepsilon(\lambda_{\text{laser}})C]^{\Gamma}(1 - \exp\{-[\gamma_1\varepsilon(\lambda_{\text{laser}})C + \varepsilon_2(\lambda_{\text{filter1}})C_2]t\})}, \tag{35}$$

which is independent of excitation intensity.

Thus, by using a single parameter, Γ, it is possible to suppress excitation intensity information from the ratio by raising one of the fluorescent emissions (dye 2 fluorescence in this case) to this value before performing the ratio computation.

As mentioned above, we implemented this approach in the measurement of thin films (of the order of 10 μm) with the use of P605 and P650 at concentrations of 8×10^{-3} and 2.4×10^{-2} mol/L of oil, respectively. Figure 17 shows the fluorescence signals at 580 and 620 nm for this mixed-dye sample in Region 1 (thin film) as obtained in Section 4. The higher excitation intensity data (40% of full power and above) have been fitted with a power regression (the results are shown in the inset of Fig. 17). In accordance with our processing scheme and Eq. (30), these data and regression suggest that the appropriate value of Γ should be close to 1.3 ($0.834/0.6512 = 1.281$, to be exact).

The fluorescence images from Region 1 validate this assumption. We obtained the ratio by using different values of Γ. The spatial intensity fluctuations should disappear from the ratio image when the proper value of Γ is used. Using values of Γ other than the proper one (either above or below it) will produce a ratio that depicts the laser's spatial intensity fluctuations because the requirements of Eq. (30) are not satisfied, as depicted in Fig. 18, which shows ratio images computed for different values of Γ. The first ratio image, which was computed for $\Gamma = 1.0$, corresponds to the original ratio that assumes a linear dependence of the fluorescent intensities on excitation intensity. It can be seen that, as the value of Γ is increased, the strength of the laser's spatial intensity fluctuations in the ratio images diminishes. An optimum is reached at a Γ value of 1.3, where the laser's spatial intensity fluctuations almost completely disappear. Further increasing the value of Γ past this point (i.e., greater than 1.3) causes the laser's spatial intensity fluctuations to appear again. Figure 19 shows a comparison of the plots of ratiovalues versus film thickness for Γ values of 1.0 (original ratio) and 1.3 (optimal value).

Before concluding, we should reiterate that this processing scheme, which is based on the power law

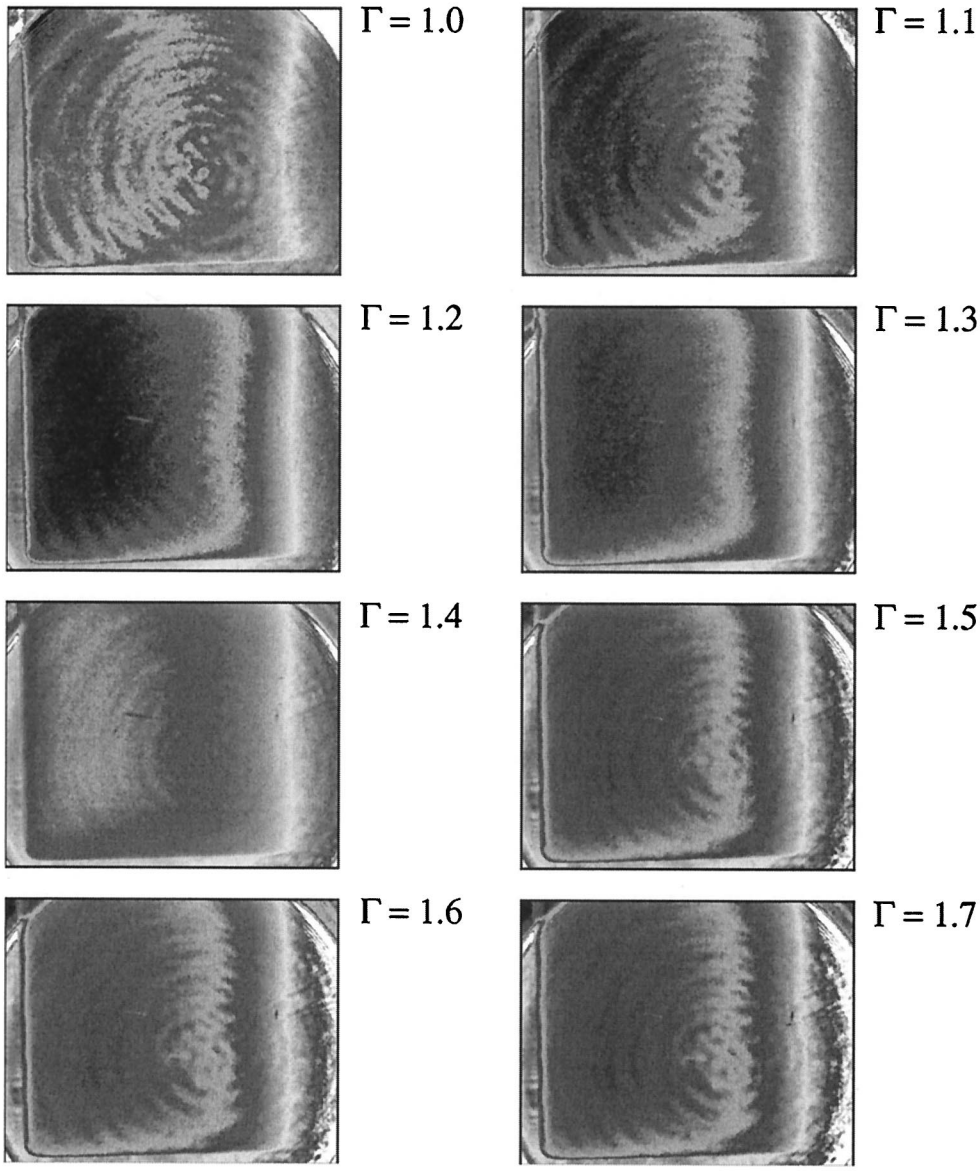

Fig. 18. Ratio images for eight values of Γ.

approximation of the fluorescence nonlinearity relative to excitation intensity, works well only for relatively small fluctuations in excitation intensity. This is so because the power law approximates the actual behavior of the fluorescent intensity curve only over a finite region of excitation intensities (Fig. 16). If the fluctuations in excitation intensity are too large, the power law will not be valid over the entire range of excitation intensity fluctuations, and the processing scheme will not suppress excitation intensity information for all values in the range of fluctuations. This is an important point to have in mind when a coherent illumination source such as a laser is used. In that case, some of the excitation source's spatial intensity fluctuations will arise as a consequence of optics-induced diffraction interference. In the far field (Fraunhofer region), the interference will become quite substantial, with the consequence that the spatial intensity fluctuations will be large between regions of constructive and destructive interference. This optics-induced diffraction interference is what gives rise to the concentric rings on the laser's spatial profile, which are appreciable in the fluorescent emission images. It is apparent that the power law assumption processing scheme eliminates the concentric rings in the ratio, which indicates that the interference is not that substantial at the location where the calibration fixture is positioned.

7. Summary and Conclusions

Emission reabsorption laser-induced fluorescence is a dual-fluorescence ratiometric technique that is capable of accurate and quasi-instantaneous two-dimensional measurements of film thickness. The core of the technique relies on the use of a ratiometric approach for the purpose of suppressing excitation

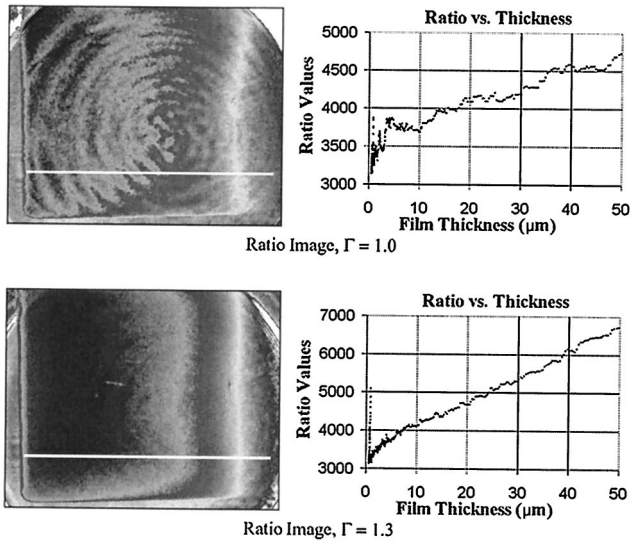

Fig. 19. Ratio images and thickness profiles for Γ values of 1.0 and 1.3.

intensity information from the fluorescent emission. Two fluorescent emissions are required for accomplishing this goal; one is used as the carrier of the desired scalar information (film thickness in this case) and the other is used as the carrier of the excitation intensity information. If the two fluorescent emissions portray the same dependence on excitation intensity, this dependence cancels in the ratio. Reabsorption of one of the fluorescent emissions, however, ensures that the behavior of the two kinds of emission with film thickness is different, preserving this information in the ratio.

If the two fluorescent emissions behave linearly with excitation intensity, the equality of dependence on excitation intensity applies, and the technique works properly. However, if the behavior of fluorescent intensities with respect to excitation intensity is nonlinear, the equality of dependences might not hold and the ratio will not properly suppress the excitation intensity. Nonlinear behavior of fluorescence with respect to excitation intensity, which is a consequence of the substantial depopulation of the ground state, is characteristic of high-excitation photon fluxes (intensities) such as those encountered in pulsed lasers. In these instances, the simple ratiometric approach will not succeed in suppressing information on the excitation intensity.

However, if the nonlinear behavior is approximated by a power law, it is possible to implement a simple scheme that will equalize the behavior of the fluorescent intensities with respect to excitation intensity. Raising one of the fluorescent emissions to the appropriate power equalizes these behaviors. In this manner it is still possible to use a ratiometric scheme to suppress information on excitation intensity. By using this technique on an appropriate fluorescence system, we have demonstrated film-thickness measurements with resolution better than 0.5 μm over a 50-μm range.

Appendix A. Nomenclature

$A \equiv 1/\tau_L$	Total excited-state transition rate constant
$A_{21} \equiv 1/\tau_{21}$	Spontaneous emission (fluorescence) rate constant
$A_{21}' \equiv 1/\tau_{21}'$	Nonradiative deactivation rate constant
A_f	Fluorescence area (pixel or photodetector area)
$B \equiv \varepsilon/N_A$	Stimulated absorption cross section
c	Speed of light
C	Molar concentration of dye; effective two-dye molar concentration
C_1	Molar concentration of dye 1
C_2	Molar concentration of dye 2
$\mathrm{d}E_f$	Differential fluorescence signal
$\mathrm{d}E_{f,1}'$	Differential fluorescence signal (reabsorption) of dye 1
$\mathrm{d}E_{f,2}$	Differential fluorescence signal (no reabsorption) of dye 2
$\mathrm{d}n$	Differential number of molecules in a differential depth slice of sample
$\mathrm{d}x$	Differential depth slice of sample
E_f	Total fluorescence signal
F_1	Excitation intensity functionality of fluorescence signal 1
F_2	Excitation intensity functionality of fluorescence signal 2
F_R	Excitation intensity functionality of ratio
G_1	Molecular properties and geometry based functionality of fluorescence signal 1
G_2	Molecular properties and geometry based functionality of fluorescence signal 2
$\hbar$	Planck's constant
$I_e \equiv \hbar\nu_{\mathrm{EX}}\rho_e$	Exciting-light intensity
I_f	Total fluorescent intensity
$I_o \equiv \hbar\nu_{\mathrm{EX}}\rho_o$	Exciting-light intensity at $x = 0$
n	Total number of molecules (ground plus excited state)
n_2	Number of molecules in excited state
N_A	Avogadro's number
R	Ratio of fluorescence signals
t	Film thickness
t_c	Thickness constant
$t_{c,1}'$	Thickness constant of fluorescence signal 1 (reabsorption)
$t_{c,2}$	Thickness constant of fluorescence signal 2 (no reabsorption)
V	Sample volume
x	Coordinate perpendicular to plane of observation
y	Coordinate parallel to plane of observation
ε	Molar absorption (extinction) coefficient; effective two-dye molar absorption (extinction) coefficient
ε_1	Molar absorption (extinction) coefficient of dye 1
ε_2	Molar absorption (extinction) coefficient of dye 2
γ	Power law exponent
γ_1	Power law exponent of fluorescence signal 1

γ_2	Power law exponent of fluorescence signal 2
Γ	Ratio of power law exponents
λ_{laser}	Laser wavelength
$\lambda_{\mathrm{filter1}}$	Wavelength of narrowband filter 1 (wavelength of fluorescence signal 1)
$\lambda_{\mathrm{filter2}}$	Wavelength of narrowband filter 2 (wavelength of fluorescence signal 2)
λ_{EM}	Emission wavelength
λ_{EX}	Excitation wavelength
$\nu_{\mathrm{EM}} \equiv c/\lambda_{\mathrm{EM}}$	Light-wave frequency of emission
$\nu_{\mathrm{EX}} \equiv c/\lambda_{\mathrm{EX}}$	Light-wave frequency of excitation
Φ	Quantum efficiency
Φ_1	Quantum efficiency of dye 1
Φ_2	Quantum efficiency of dye 2
ρ_c	Excitation photon flux constant
ρ_e	Excitation photon flux
ρ_{o}	Excitation photon flux at $x = 0$
τ	Time
τ_{21}	Spontaneous emission (fluorescence) lifetime
τ_{21}'	Nonradiative deactivation lifetime
τ_e	Photodetector exposure time
τ_L	Combined excited-state lifetime (fluorescence and nonradiative)
τ_p	Laser pulse width

References

1. H. Ayala, D. P. Hart, O. Yeh, and M. C. Boyce, "Wear of oil containment elastomer in abrasive slurries," Wear **220,** 9–21 (1998).
2. A. Y. Joffe, V. F. Sayenko, N. A. Denisov, S. M. Dets, and A. N. Buryi, "Early diagnosis of gastric cancer with laser induced fluorescence," in *Optical and Imaging Techniques for Biomonitoring IV*, M. Dal Fante, H.-J. Foth, N. Krasner, R. Marchesini, and H. Podbielska, eds., Proc. SPIE **3567,** 10–17 (1999).
3. N. Georgiev and M. Alden, "Two-dimensional imaging of flame species using two-photon laser-induced fluorescence," Appl. Spectrosc. **51,** 1229–1237 (1997).
4. A. Kovacs, "Visualization of fuel-lubricant on the cylinder surface in the combustion chamber of SI engines," Lubr. Sci. **7,** 149–162 (1995).
5. B. Thirouard and D. P. Hart, "Investigation of oil transport mechanisms in the piston ring pack of a single-cylinder diesel engine, using two-dimensional laser induced fluorescence," J. Fuels Lubr. **107,** 2007–2015 (1998).
6. J. Coppeta and C. Rogers, "Dual emission laser induced fluorescence for direct planar scalar behavior measurements," Exp. Fluids **25,** 1–15 (1998).
7. J. Sakakibara and R. J. Adrian, "Whole field measurement of temperature in water using two-color laser induced fluorescence," Exp. Fluids **26,** 7–15 (1999).
8. C. H. Hidrovo and D. P. Hart, "Emission reabsorption laser induced fluorescence (ERLIF) film thickness measurement," Meas. Sci. Technol. **12,** 467–477 (2001).
9. V. I. Yushakov, K. G. Yevsyukhina, and S. V. Patsayeva, "Laser induced saturation of fluorescence for complex organic molecules," in *ALT'97 International Conference on Laser Surface Processing*, V. I. Pustovoy, ed., Proc. SPIE **3404,** 388–396 (1997).
10. S. Patsayeva, V. Yuzhakov, and V. Varlamov, "Laser induced fluorescence saturation for binary mixtures of organic luminophores," in *ICONO '98 Laser Spectroscopy and Optical Diagnostics: Novel Trends and Applications in Laser Chemistry, Biophysics, and Biomedicine*, A. Y. Chikishev, V. N. Zadkov, and A. M. Zheltikov, eds., Proc. SPIE **3732,** 147–156 (1999).
11. D. P. Hart, "Super-resolution PIV by recursive local-correlation," J. Visualization **3,** 187–194 (2000).
12. G. Georgiev, T. Kalkanjiev, D. Metchkov, Zh. Nickolov, and K. Stamenov, "Influence of the shape of the exciting laser pulse on fluorescence saturation in the quantitative analysis of dissolved trace organic substances," J. Lumin. **27,** 89–99 (1982).
13. S. Saeki and D. P. Hart, "Investigation on YAG (532) laser dyes for oil film thickness and temperature measurement," in *Proceedings of the 3rd Pacific Symposium on Flow Visualization and Image Processing*, T. Kobayashi, ed. (T. Kobayashi, Tokyo, Japan, 2001), available on CD-ROM.
14. G. Jones, II, Z. Huang, S. Kumar, and D. Pacheco, "Fluorescence and lasing properties of benzo-fused pyrromethene dyes in poly(methyl methacrylate) solid host media," in *Solid State Lasers XI*, R. Scheps, ed., Proc. SPIE **4630,** 65–74 (2002).
15. H. Dornauf and J. Heber, "Concentration-dependent fluorescence quenching in $La_{1-x}Pr_xP_5O_{14}$," J. Lumin. **22,** 1–16 (1980).
16. A. P. Losev, ´E. I. Zen'kevich, and E. I. Sagun, "Concentration quenching of fluorescence and triplet formation of chlorophyll *a* and pheophytin in solutions," J. Appl. Spectrosc. **27,** 996–998 (1977).
17. R. Y. Tsien and A. Waggoner, "Fluorophores for confocal microscopy: photophysics and photochemistry," in *Handbook of Biological Confocal Microscopy*, 2nd ed., J. B. Pawley, ed. (Plenum, New York, 1995), pp. 267–279.
18. T. Hirschfeld, "Quantum efficiency independence of the time integrated emission from a fluorescent molecule," Appl. Opt. **15,** 3135–3139 (1976).
19. C. H. Hidrovo, "Development of a fluorescence based optical diagnostics technique and investigation of particle ingestion and accumulation in the contact region of rotating shaft seals," Ph.D. dissertation (Massachusetts Institute of Technology, Cambridge, Mass., 2001).